C: Physical Processes in Nanomaterials and Nanostructures

The Effects of Radius and Length on the Nanomotor Rotors in Aqueous Solution Driven by the Rotating Electric Field

Zhongyu Fu, Dong Liang, Shuanlei Jiang, Pengde Zhao, Kaixin Han, and Zhen Xu

J. Phys. Chem. C, **Just Accepted Manuscript** • DOI: 10.1021/acs.jpcc.9b07345 • Publication Date (Web): 25 Nov 2019

The Effects of Radius and Length on the Nanomotor Rotors in Aqueous Solution Driven by the Rotating Electric Field

Zhongyu Fu[1], Dong Liang[1], Shuanlei Jiang[1], Pengde Zhao[1], Kaixin Han[2], Zhen Xu[1,*]

[1]*School of Mechanical and Automotive Engineering, Shanghai University of Engineering Science, Shanghai 201620, China.*

[2]*School of Mechanical Engineering, University of Shanghai for Science and Technology, Shanghai 200093, China.*

* Corresponding author: Zhen Xu, E-mail address: lcxuzhen@163.com

Abstract: The nanomotors with ultra-high speed that are easy to assemble, with low friction and long service life, have been actively researched in several fields recently, owing to the relentless development of nanoelectromechanical systems (NEMS). Based on the principle that the reorientation of the water dipole moment induced by the rotating electric field can rotate the carbon nanotubes (CNTs) immersed in the aqueous solution. The dynamic behaviors of nanomotor rotors with different radii and lengths are studied. According to molecular dynamics (MD) simulations, the lag angle between the nanomotor rotor and the water molecule dipole can be reduced by increasing the radius of the nanomotor rotor or increasing the length of the nanomotor rotor. At the same time, the synchronization speed between the nanomotor rotor and the rotating electric field can also be increased by increasing the radius of the nanomotor or reducing the length of the nanomotor rotor. These studies show that the radii and lengths of the nanomotor rotor can affect the nanomotor rotor rotation angle, rotation speed and cycle time. Our findings may have potential applications in the design of nano-propellers and nanogears of complex structure.

1. Introduction

The inevitable transition of motors[1, 2] from microelectromechanical systems (MEMS)[3] to NEMS,[4] besides the continuous development of nanotechnology and electromechanical systems, has been actively researched in recent years.

Nanomotors[5-13] are nanoscale devices capable of producing linear and (or) rotational motion. Recently, there are certain accomplishments on driving nanomotors through various methods in non-solution environment.[14-17] For e.g., Wang *et al.*[16] developed an ultrasound-driven DC nanomotor. The nanomotor has a good response to ultrasound and can collect and convert energy from the surrounding environment. Barreiro *et al.*[17] designed a nanofabricated motor which could realize micro-nano feed in both the longitudinal and transverse directions, utilizing the inverse piezoelectric effect of piezoelectric ceramics. These potential applications are relevant in the fields of optics and microelectronic design and

manufacturing.

Despite several achievements on nanomotors in non-solution environment, the studies over the precise control of nanomotors in aqueous solution are sparse. Owing to the peculiar properties of CNTs,[18-23] CNT-based nanomotors in liquid environment have become an important research field in NEMS in recent years.[16, 24-26] According to the investigations on the orientation mechanisms of CNTs by Guo *et al*.,[24] when an electric field is applied, the water molecule dipoles align with the electric field and the CNT is then forced to align its surface with the electric field, which sets the basis for applying an electric field to drive CNT motor rotors in water. Wang *et al.*[16] reported a liquid pump (nano-propeller) synthesized by CNTs and pyrene molecules, and performed MD simulation on the pumping rate of the liquid pump. However, the motor system employed to drive the nano-propeller has not been demonstrated unambiguously. Owing to the lack of clear illustration of the nanomotor systems, the design of nanomotor rotor systems in aqueous solution and the nanogear system to drive external loads might become difficult. Based on the principle that CNTs immersed in an aqueous solution can be rotated through the orientation of water dipole moment under the induction of rotating electric field, Rahman *et al*.[25] designed a single molecule bladed propeller and simulated the nanogear system that drives the external load. However, the effects of radii and lengths on the dynamic behaviors of nanomotor rotors have not been analyzed in detail.

Based on the previously mentioned studies, this work is divided into two parts. First, (8,8), (10,10), (12,12), (14,14) and (16,16) armchair CNTs with a length of 7 nm and good symmetry are selected as a nanomotor rotor.[27-31] Next, (10,10) type CNTs for different lengths of 4, 7, 10, 13 and 15 nm are used as the nanomotor rotor. MD simulations of nanomotor systems in aqueous solution are performed using MD methods. The effects of the nanomotor rotors with different radii and lengths on rotor speed, rotation angle and period of nanomotors are studied. This study provides an important theoretical reference for the design of nano-water pumps, nano-propellers, and nanogears. It also sets the foundation for the development of NEMS for physics, chemistry, biology, and environment related fluids.

2. Modelling and Numerical Method

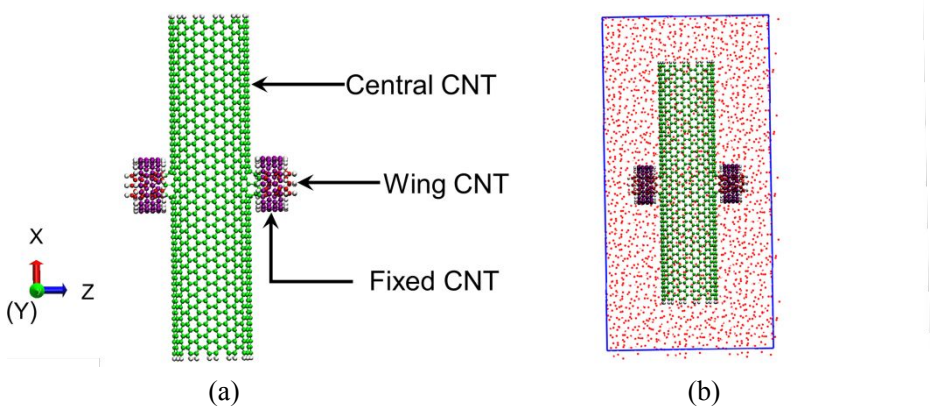

(a) (b)

Figure 1. (a) The atomic structure of the nanomotor (the green part represents the nanomotor rotor (central CNT), the red part represents the wing CNTs of the nanomotor, the purple part represents the fixed CNT used to fix the nanomotor rotor, and the white indicates a hydrogen atom used to saturate the carbon atoms), and (b) a nanomotor immersed in aqueous solution.

Figure 1(a) shows an atomic structure model of the proposed nanomotor, and Fig. 1(b) shows a nanomotor immersed in an aqueous solution. In order to saturate the carbon atoms at the edge of the rotor, hydrogen atoms are added in the vicinity of them. To ensure two wing CNTs on the sides of the nanomotor rotor aligned on the same axis, (8,8), (10,10), (12,12), (14,14) and (16,16) CNTs with good symmetry and length 7.0 nm are selected as the rotor of the nanomotor. The two wing CNTs of chirality (6,0) and length 0.93 nm are used as the rotating shaft of the nanomotor, which can rotate with the motor rotor. The wing CNTs are placed in the center of the two fixed CNTs of chirality (8,8) and length 0.59 nm. These fixed CNTs are used as a stator of the nanomotor and do not rotate with the motor rotor. The fixed CNTs support the nanomotor shaft and ensure smooth operation of the motor rotor. Wing CNTs and fixed CNTs of the same size and chirality are used in five different radii nanomotor rotor systems. As the rotor radius increases, the relative positions of the wing CNTs and the fixed CNTs are adjusted. In addition, (10,10) type CNTs with 4, 7, 10, 13 and 15 nm are used as the rotor of the nanomotor. Two wing CNTs of chirality (6,0) and length 0.93 nm are mounted on the sides of the nanomotor rotor with different lengths. The two wing CNTs serve as the rotating shaft of the nanomotor and are attached to the outside of the motor rotor. Since this part only modifies the length of the rotor, the relative position of the nanomotor system with different lengths in the *Z* axis direction does not change. Therefore, the same coordinate position parameters can be used for the wing CNTs and the fixed CNTs attached to both sides of the rotor of the nanomotor with different lengths. Due to the effect of the van der Waals (vdW) forces, the frictional wear between the wing CNTs and water molecules, as well as that between the wing CNTs and the fixed CNTs, is lower. Thereby, the service life of the nanomotor has a longer durability. In real environments, fixed CNTs require mounting

on some rigid support device.

The *XY* plane is set as the rotation plane of the nanomotor and the rotating electric fields on the *X* and *Y* axes are constructed (the rotation can be realized when the two rotating electric fields are overlapped). The functional form for the rotating electric fields are $Ex=Et\cdot cos(\omega t)$ and $Ey=Et\cdot sin(\omega t)$, where *Ex* and *Ey* represent the field strength after the composite computation, *Et* represents the initial electric field strength of the rotating electric field, ω represents the angular speed of the rotating electric field, and *t* represents the time over which the rotating electric field changes. In practice, the rotating electric field can be constructed by adjusting the phase angle of the alternating current.

The MD simulations are performed by employing GROMACS 5.1.4.[26, 32] The ensemble for the simulation is NVT, i.e., the number of atoms, volume, and temperature remain constant. The Rescaling Velocity Method (V-rescale) is used to maintain the temperature at around 300 K. Furthermore, the transferable intermolecular potential three-point (TIP3P) water model is used during the simulation process with the Lennard-Jones (LJ) parameters at $\sigma_{cc} = 0.34\ nm$ and $\varepsilon_{cc} = 0.3664\ KJ \cdot mol^{-1}$.[26, 33-35] The equilibrium bond length between the carbon atoms is 0.1418 nm. The Harmonic potential energy function is used to constrain the bonds, where the constrained energy coefficients are 393960 kJ•mol^{-1} and 527 kJ•mol^{-1}•rad^{-2}, respectively. Furthermore, a relatively weak value of regular dihedral potential energy is applied to constrain the vibration of the carbon-carbon bonds. The LJ potential energy between the carbon and oxygen atoms is used to describe the interaction between CNTs and water molecules, and the LJ parameters are $\sigma_{co} = 0.3275\ nm$, $\varepsilon_{co} = 0.4772\ KJ \cdot mol^{-1}$. The parameters for the current research have been extensively applied in previous studies.[36-38]

The truncated algorithm is used for LJ potential energy during the simulation with a truncation radius of 1 nm. The electrostatic interaction is subjected to Particle-Mesh-Ewald (PME) algorithm,[26, 39] where the truncation radius for short-range action is 1 nm, the time step is 2 fs, and the data sampling frequency is one frame per 0.5 ps. The method of steepest descent is applied to minimize the energy in the initial system.

3. Results and Discussion

According to Bratko *et al.*,[40] the electric field can change the hydrophobicity of the graphene surface to be hydrophilic. When an electric field is applied, the water molecules are optimized for hydrogen bonding

and tend to be parallel to the graphene interface. When the water molecules are parallel to the direction of the electric field, the number of hydrogen bonds at the graphene interface is maximized. The combination effect of the confined interface and the electric field provides the driving force for the graphene orientation in water. As reported by Xu *et al*.,[41] when the dipoles of water molecules on the CNT surface are parallel to the direction of the electric field, the hydrogen bond density is large, and more hydrogen bonds are formed. When the electric field is perpendicular to the dipole of the water molecule on the CNT surface, the hydrogen bond density is small, and less hydrogen bonds are formed. According to Guo *et al*.,[24] when an electric field is applied, the CNT is forced to align its surface toward the dipole orientation of the water molecules to maximize the hydrogen bonds. To meet these two requirements, the CNT forces its surface to be consistent with the direction of the electric field. Therefore, the CNTs in the aqueous solution can achieve the effect of rotation under the induction of a rotating electric field.

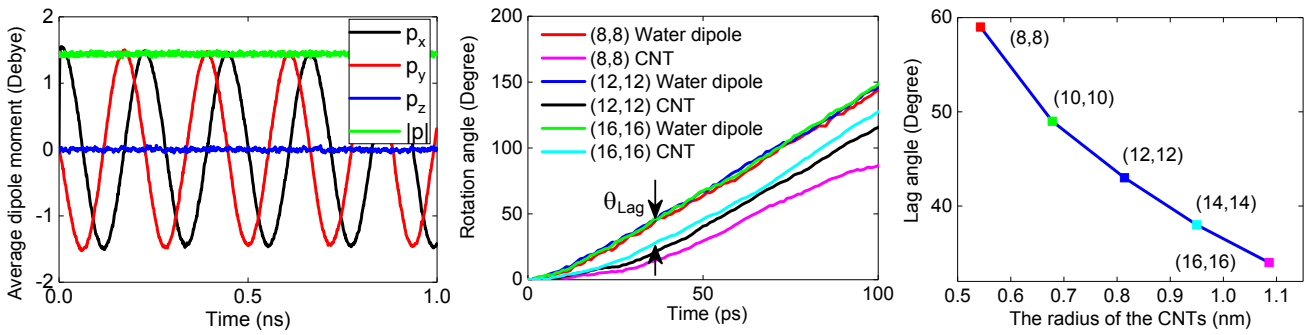

(a) (b) (c)

Figure 2. (a) The variation curve of the average dipole moment of water molecules versus time along the *X*, *Y*, and *Z* axes in the (12,12) nanomotor system, with a rotating electric field strength of 1v/nm and speed of 2.75×10^{11} rpm, (b) the variation curves of the rotation angles of water dipole and motor rotor versus time during the rotation of the nanomotor rotors of type (8,8), (12,12) and (16,16), with a rotating electric field strength of 1v/nm and speed of 2.75×10^{11} rpm, and (c) the variation curve of the lag angle of the motor rotor relative to water molecule dipoles versus the radius of the CNTs.

The average dipole moment curves of water molecules along the *X*, *Y* and *Z* axes in the (12,12) nanomotor system are selected as an example in Figure 2(a), where the phase difference between p_x and p_y is 90°. The variation curves of p_x and p_y versus time are satisfied with the cosine and sine rules, which are consistent with the changes in the constructed rotating electric field function. As for the p_z curve, it is related to the rotation plane. Owing to the variation of the electric field strength along the *XY* plane, the orientation of the water molecule dipoles tends to coincide with the direction of the electric field. Furthermore, under the action of vdW force, the orientation of the water molecule dipoles may deviate from the *XY* plane at times. Therefore, the value of p_z fluctuates around zero.

Because the rotation of the nanomotor rotor in aqueous solution in the electric field is driven by the guiding effect of water molecule dipoles, the rotation mechanism of different nanomotor rotors is identical. The (8,8), (12,12) and (16,16) nanomotor rotors are selected as examples to draw the corresponding rotation angle curves [Figure 2(b)] for convenient observation. The lag angle between the rotor and water molecule dipole is noted as θ_{Lag}. This is an easier method to identify the influence of rotor radius on the nanomotor. The rotation angle is the angle accumulated by the motor rotor relative to the initial position during the rotation. As the radius of the rotor increases, the rotation angle curve of water molecule dipoles does not change significantly, but the rotation angle of the rotor is constantly increasing [Figure 2(b)]. When the strength of the rotating electric field is 1v/nm with a speed of 2.75×10^{11} rpm, the lag angles of the (8,8), (10,10), (12,12), (14,14) and (16,16) nanomotor rotors relative to the water molecule dipoles are 59°, 49°, 43°, 38° and 34°, respectively. Figure 2(c) represents the variation curve of lag angle versus the radius of CNT. It is obvious that as the rotor radius increases, the lag angle decreases. This is mainly because as the radius of the motor rotor increases, the inner and outer surfaces of the CNTs per unit area can contact more water molecules, which strengthens the guiding role of water molecules. As reported by Zasetsky *et al*.,[42] when the rotational speed of the applied electric field is sufficiently low, the rotation angle of CNTs and water molecule dipoles is almost synchronous. In addition, when the speed of the electric field exceeds a certain value, a lag angle appears between the rotation angle of CNTs and water molecule dipoles. Therefore, the approach of increasing the radius of the motor rotor needs to be considered to reduce the lag angle between the motor rotor and the water molecule dipoles.

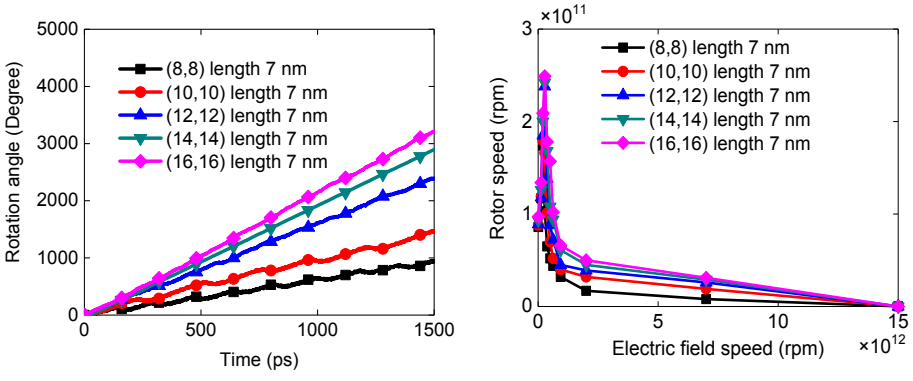

(a) (b)

Figure 3. (a) The rotation angle variation curves of nanomotor rotors with different radii versus time, with a rotating electric field strength of 1v/nm and speed of 2.75×10^{11} rpm, and (b) the rotor speed variation curves of nanomotor rotors with different radii versus electric field speed.

The average speed of the nanomotor rotor in one cycle represents the rotational speed. It can be seen

from Figure 3(a) that for the nanomotor rotors with different radii, the rotation angle of the rotor enlarges during the rotation with the increase of the nanomotor rotor radius. The rotation angle curves of (8,8) and (10,10) nanomotor rotors increase with fluctuation, whereas that of (12,12), (14,14) and (16,16) nanomotor rotors have a tendency for linear growth. This is because the electric field speed exceeds the synchronous speed that the motor rotor is capable of, which results in the continuous and periodic back and forth movement during rotation (see Movie S1 and Movie S2 in the Supporting Information). When the electric field speed is 2.75×10^{11} rpm, the (8,8) and (10,10) nanomotor rotors fail to keep up with the rotating electric field, which results in back and forth movement during the rotation. However, the (12,12), (14,14) and (16,16) nanomotor rotors can "lock" with the electric field speed under the identical conditions, and move in any angle in tandem with the rotating electric field (see Movie S3 and Movie S4 in the Supporting Information). Therefore, the effect of the rotor radius on the motor rotor speed is taken into account. This consideration is to avoid the back and forth movement of the nanomotor rotor during rotation. By adjusting the rotor radius of the motor, the nanomotor system with higher efficiency can be designed.

As illustrated by Figure 3(b), when the electric field speed approaches within the range of 7×10^{12} ~15×10^{12} rpm, the speed of all the nanomotor rotors with different radii plummets to near zero, owing to the nanomotor rotor failing to tandem with the electric field at very high speeds. This agrees with the reports of Rahman *et al*.[25] and Zasetsky *et al*.[42] that not all electric fields with any speed can feasibly drive the nanomotor rotors. Furthermore, the speed of the nanomotor rotors with different radii increases to a specific point along with the electric field speed before manifesting a downward trend. For the (8,8) and (10,10) nanomotor rotors, the turning point is 2×10^{11} rpm (electric field speed), whereas that for the (12,12), (14,14) and (16,16) nanomotor rotors is 2.75×10^{11} rpm (electric field speed). Therefore, it can be seen that the turning point of the rotor speed changes for nanomotors with different radii. This owes to relatively more water molecules being contained in the rotor as the radius increases, which leads to an enhanced guiding effect from the water molecule dipoles. Thus, when a rotating electric field is applied, a larger radius nanomotor rotor system can achieve higher rotational speeds. However, as the radius of the nanomotor rotor becomes larger, the moment of inertia of the system also becomes larger. At the same time, the frictional wear between the nanomotor rotor and water molecules, as well as that between the wing CNTs and the fixed CNTs, is exacerbated. For a larger radius nanomotor rotor, the speed of the motor rotor can be maximized by increasing the speed of the rotating electric field.

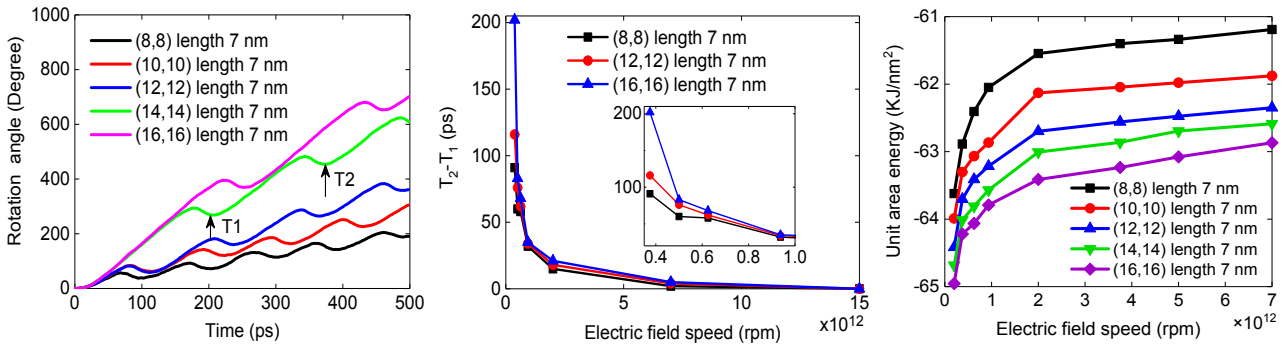

(a) (b) (c)

Figure 4. (a) The variation curves of rotation angle of nanomotor rotors with different radii versus time, with a rotating electric field strength of 1v/nm and speed of 3.75×10^{11} rpm, (b) the variation curves of lag time of nanomotor rotors with three different radii versus electric field speed, and (c) the variation curve of the unit area interaction energy between the nanomotor rotor with different radii and the aqueous solution versus the electric field speed.

After analyzing Figure 3(a), the back and forth movement occurs in all the nanomotor rotors with different radii. Therefore, an electric field strength of 1v/nm and an angular speed of 3.75×10^{11} rpm, when all the nanomotor rotors of different radii would move back and forth, are selected for further analysis. The lag time ($t = T_2 - T_1$) is used to measure the back and forth movement of the nanomotor rotors. According to Figure 4(a), the lag time of the (8,8), (10,10), (12,12), (14,14) and (16,16) nanomotor rotors is 97, 102, 131, 171 and 208 ps, respectively. Hence, the calculation shows that the lag time increases as the radius of the nanomotor rotors enlarges. The simulations show that the variation of the lag time of the nanomotor rotors with different radii is basically identical. Thus, the (8,8), (12,12) and (16,16) nanomotor rotors are selected as the study objects. As shown in Figure 4(b), the lag time increases as a whole for the nanomotor rotors with larger radius. It can be seen from the inset of Figure 4(b) that when the electric field speed is in range of 0.4×10^{12} to 1×10^{12} rpm, the speed of the rotor changes more significantly. Therefore, the rotational electric field of the range can be used to adjust the rotational speed of the motor rotor system to achieve precise control of the motor rotor system. The lag time of each nanomotor rotor declines as the electric field speed increases, which is in accordance with the conclusion drawn by Rahman *et al.*[25] As shown in Figure 3(b), when the electric field speed is sufficiently high, the rotor speed of the nanomotor cannot keep up with the electric field speed, and the rotational motion of the motor rotor is stopped. The proportion of the lag time in the entire cycle reduces as the rotation period of the nanomotor rotor extends.

Figure 4(c) shows the variation of the interaction energy per unit area between the nanomotor rotor and the aqueous solution. The interaction energy per unit area is equal to the interaction energy between the rotor and the aqueous solution divided by the surface area of the rotor. According to Figure 4(c), the

unit area interaction energy between the rotor and the aqueous solution is enhanced at a specific electric field speed. Therefore, the method of changing the radius of the motor rotor can be applied for the design of the nanomotor rotor system to enhance the orientation degree of the water molecules, which also shortens the orientation time of the water molecules surrounding the nanomotor. Furthermore, it can enhance the driving of the motor rotor by the water molecules in a shorter time.

Since the rotation angle curves of the water molecule dipole and the motor rotor are consistent in the nanomotor system with different lengths, the nanomotor rotor curves of 4, 10 and 15 nm are selected for analysis [Figure 5(a)]. It can be seen that the lag angle between the water molecule dipole moment and the motor rotor is different for the nanomotor system with different lengths. As shown in Figure 5(b), the lag angles of the nanomotor rotors of 4, 7, 10, 13 and 15 nm are 68°, 49°, 42°, 36° and 32°, respectively. It can be obviously seen in Figure 5(b) that as the rotor length increases, the lag angle of the rotors with different lengths decreases. Figure 5(c) shows that the 4 nm long motor rotor has a large angular change relative to other length motor rotors at the same time. As the length of the nanomotor rotor increases, the motor rotor rotation angle decreases. Combined with Figure 5(b) and Figure 5(c), although the 4 nm long nanomotor rotor has a relatively large lag angle, the rotational angle is the largest. The 15 nm long motor rotor has a small lag angle, while the rotational angle is the smallest. Therefore, when designing a nanomotor rotor, it is not preferable to reduce the lag angle of the motor rotor by lengthening the rotor length. Choosing suitable length of nanomotor rotor can not only improve the speed of the rotor, but also carry other loads to work properly, thus improving the efficiency of the nanomotor.

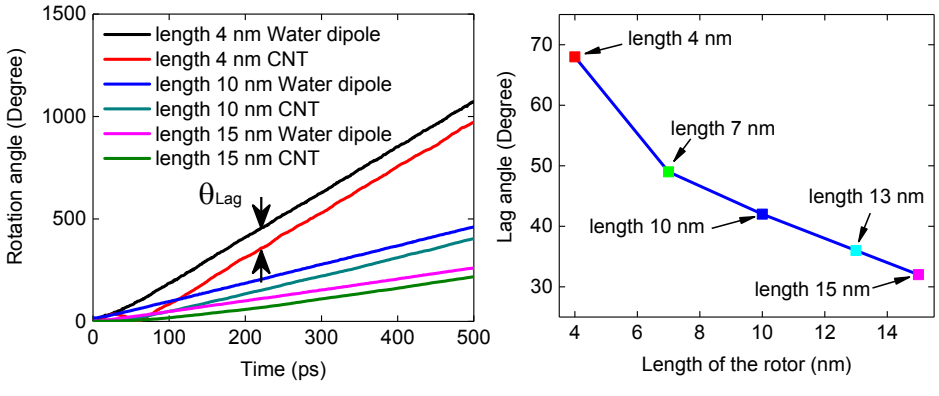

(a) (b)

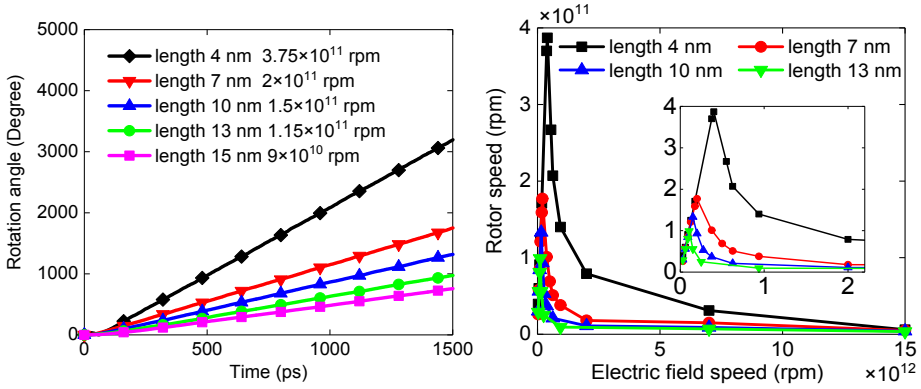

(c) (d)

Figure 5. (a) The dipole and the motor rotor rotation angle curves as the function of time when the rotating electric field strength is 1 v/nm, and the speed of motor rotors with 4, 10 and 15 nm is corresponding to 3.75×10^{11}, 1.5×10^{11}, 9×10^{10} rpm, respectively, (b) the variation curve of the lag angle versus the length of the rotor of the motor when the rotating electric field strength is 1 v/nm, and the speed of motor rotors with 4, 7, 10, 13 and 15 nm is corresponding to 3.75×10^{11}, 2×10^{11}, 1.5×10^{11}, 1.15×10^{11}, 9×10^{10} rpm, respectively, (c) when the rotating electric field strength is 1 v/nm and the motor rotor has no back and forth movement, the rotation angle of the rotor with different lengths is changed with respect to time, and (d) when the field strength is 1 v/nm, the relationship between the rotor speed of different lengths of nanomotors and the rotational electric field speed.

Figure 5(d) shows the variation of the rotor speed of different length nanomotors with the rotating electric field speed. Since the rotor motor speed curves of different lengths have the same trend, all rise to a certain value and then fall. For the convenience of observation, nanomotor rotors with lengths of 4, 7, 10 and 13 nm are selected as observation objects. In Figure 5(d), it can be found that when the rotational electric field speed is in range of 7×10^{12} to 15×10^{12} rpm, the motor rotor speed drops sharply to zero for the nanomotor rotor with different lengths. The nanomotor rotor cannot follow the electric field when the rotating electric field is too fast, which agrees with the results of Rahman *et al*.[25] and Zasetkey *et al*.[42] It can be seen from the inset of Figure 5(d) that when the rotational electric field speed is less than 1×10^{12} rpm, the change of the rotor speed curve is more obvious. The maximum rotor speeds of nanomotors with lengths of 4, 7, 10, 13 and 15 nm are 3.7×10^{11}, 1.77×10^{11}, 1.33×10^{11}, 9.9×10^{10} and 7.8×10^{10} rpm, respectively. Comparing Figure 5(c) and Figure 5(d), it can be found that the rotational electric field speed applied to the system is not exactly equal to the rotational speed of the output nanomotor rotor. The result demonstrates that the frictional wear between the rotor and the aqueous solution is affected by the length of the nanomotor rotor.

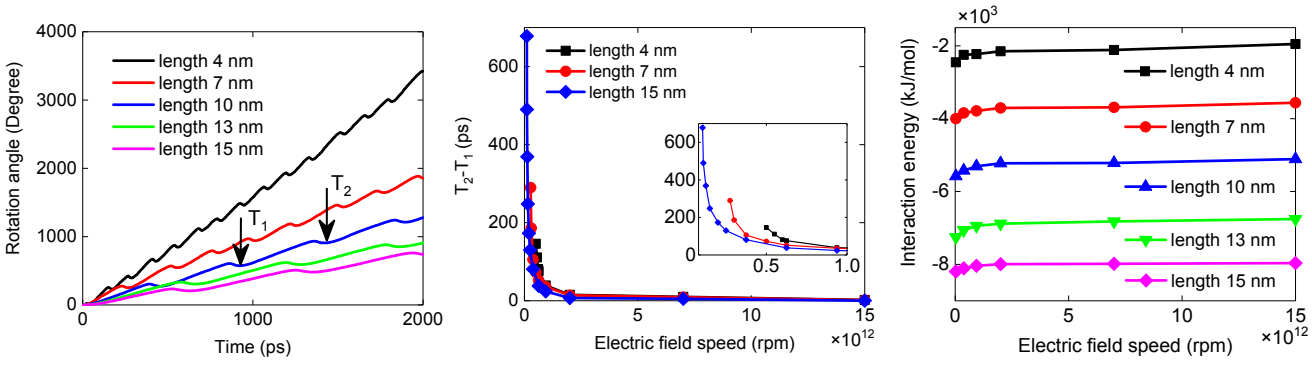

(a) (b) (c)

Figure 6. (a) The rotation angle curve of the nanomotor rotor with different lengths when the rotating electric field strength is 1 v/nm, and the speeds of motor rotors with 4, 7, 10, 13 and 15 nm are corresponding to 5×10^{11}, 3×10^{11}, 2×10^{11}, 1.5×10^{11}, 1×10^{11} rpm, respectively, (b) the variation of the lag time of different length nanomotor rotors with the rotating electric field speed, and (c) variation curves of interaction energy between motor rotor with different lengths and aqueous solution.

The rotation curve of the motor rotor is shown in Figure 6(a) when the nanomotor rotors with different lengths produce back and forth movement. Figure 6(b) shows the variation of the lag time when the back and forth movements of nanomotor rotors with different lengths occur at different rotational electric field speeds. It can be seen in Figure 6(b) that as the length of the nanomotor rotor increases, the speed of the rotating electric field decreases when the rotor has a lag time [in the inset in Figure 6(b), the electric field speed in the range of 8×10^{10} to 1×10^{12} rpm is selected to illustrate]. According to Figure 5(d), it can be seen that when the speed of the rotating electric field exceeds a certain value, the speed of the nanomotor rotors with different lengths tends to decrease. The speed of the rotating electric field is too fast for the nanomotor rotor to keep up with the pace of the rotating electric field, which results in a stagnant state. This makes the rotation period of the nanomotor rotor longer, and the proportion of the lag time in the entire cycle becomes smaller and smaller.

Figure 6(c) shows the variation of the interaction energy between the nanomotor rotors with different lengths and the aqueous solution. As can be seen from Figure 6(c), the rotor interaction energy for the same length of nanomotor rotor increases as the rotational electric field speed increases. This trend is consistent with the conclusions of Guo *et al.*[24] and Winarto *et al.*[43] that a higher rotating electric field causes a higher degree of orientation of water molecules around the nanomotor. It is obvious that the interaction energy of the 4 nm long nanomotor rotor are overall larger than that of other nanomotor with different lengths. Therefore, the 4 nm long nanomotor rotor can be oriented in a shorter time. From the perspective of the

rotation effect, the 4 nm long nanomotor rotor has a larger rotation angle than the other rotors. Therefore, when designing a nanomotor rotor, the effect of length on the interaction energy of the nanomotor rotor needs to be taken into account. By changing the length of the nanomotor rotor, the interaction energy between the rotor and the water molecules is improved, and the orientation time of the water molecules around the nanomotor is shortened.

In summary, according to the analysis of the results of nanomotor rotors with different lengths, it can be known that the lag angle can be reduced by increasing the length, so that the nanomotor rotor can be consistent with the dipole moment orientation of the water molecules in a short time. However, if the length of the nanomotor rotor is too long, although the lag angle is small, the frictional wear between the excessively long nanomotor rotor and the aqueous solution increases. In addition, the moment of inertia of the motor rotor itself increases as the length of the rotor grows. These factors will be detrimental to the rapid rotation of the nanomotor rotor. If the length of the nanomotor rotor is too small, although the rotation angle will increase, the ultra-small nanomotor will not be able to carry the load.

4. Conclusions

The nanomotors in aqueous solution driven by the rotating electric field designed in the current research have the advantages of easy assembly and low friction. According to the MD simulations of the nanomotor rotor with different radii and lengths, the lag angle can be reduced by increasing the radius of the nanomotor rotor or increasing the length of the rotor at an appropriate electric field speed. What's more, the synchronization speed between the nanomotor rotor and the rotating electric field can also be improved by increasing the radius of the nanomotor or reducing the length of the nanomotor rotor. However, excessively increasing the radius of the nanomotor or lengthening the nanomotor rotor increases the inertia moment of the nanomotor itself and does not accelerate the effect of its own motion.

The nanomotor rotors with different radii and lengths provide design parameters for future research on nanomotors carrying loads. This research has given us a deeper understanding of the nanomotor structures and helps to further improve the design of nanomotors. Structurally complex devices such as nano-rotary pumps, novel nanofluidic devices, and nano-automobiles controlled by rotating electric fields can be further improved by adjusting the radius or length of the rotor.

Supporting Information

The following are available online at:

https://github.com/fzypaper/hello_world.git
Movie-S1.mp4
Movie-S2.mp4
Movie-S3.mp4
Movie-S4.mp4

Acknowledgment

This work was supported by the National Science Foundation of China, (Grant No. 11604203).

References

(1) Zhang, X.; Guo, Q.; Cui, D. Recent Advances in Nanotechnology Applied to Biosensors. *Sensors* **2009**, *9*, 1033-1053.
(2) Guix, M.; Mayorga-Martinez, C. C.; Merkoçi, A. Nano/Micromotors in (Bio)Chemical Science Applications. *Chem. Rev.* **2014**, *114*, 6285-6322.
(3) Judy, J. W. Microelectromechanical Systems (Mems): Fabrication, Design and Applications. *Smart Materials and Structures* **2001**, *10*, 1115-1134.
(4) Ekinci, K. L.; Roukes, M. L. Nanoelectromechanical Systems. *Science* **2005**, *76*, 25-30.
(5) Li, J. J.; Tan, W. A Single DNA Molecule Nanomotor. *Nano Lett.* **2002**, *2*, 315-318.
(6) Fennimore, A. M.; Yuzvinsky, T. D.; Han, W. Q.; Fuhrer, M. S.; Cumings, J.; Zettl, A. Rotational Actuators Based on Carbon Nanotubes. *Nature* **2003**, *424*, 408-410.
(7) Balzani, V.; ClementeLeón, M.; Credi, A.; Ferrer, B.; Venturi, M.; Flood, A. H.; Stoddart, J. F. Autonomous Artificial Nanomotor Powered by Sunlight. *P. Natl. Acad. Sci. USA.* **2006**, *103*, 1178-1183.
(8) Eelkema, R.; Pollard, M. M.; Vicario, J.; Katsonis, N.; Ramon, B. S.; Bastiaansen, C. M.; Broer, D. J.; Feringa, B. L. Nanomotor Rotates Microscale Objects. *Nature* **2015**, *440*, 163.
(9) Bishop, J. D.; Klavins, E. An Improved Autonomous DNA Nanomotor. *Nano Lett.* **2007**, *7*, 2574-2577.
(10) Zambrano, H. A.; Walther, J. H.; Jaffe, R. L. Thermally Driven Molecular Linear Motors: A Molecular Dynamics Study. *J. Chem. Phys.* **2009**, *131*, 241104.
(11) Klapper, Y.; Sinha, N.; Ng, T. W. S.; Lubrich, D. A Rotational DNA Nanomotor Driven by an Externally Controlled Electric Field. *Small* **2010**, *6*, 44-47.
(12) Chen, Y.; Shi, Y. Characterizing the Autonomous Motions of Linear Catalytic Nanomotors Using Molecular Dynamics Simulations. *J. Phys. Chem. C* **2011**, *115*, 19588-19597.
(13) Li, J.; Gao, W.; Dong, R.; Pei, A.; Sattayasamitsathit, S.; Wang, J. Nanomotor Lithography. *Nat. Commun.* **2014**, *5*, 5026.
(14) Kim, K.; Xu, X.; Guo, J.; Fan, D. L. Ultrahigh-Speed Rotating Nanoelectromechanical System Devices Assembled from Nanoscale Building Blocks. *Nat. Commun.* **2014**, *5*, 3632.
(15) Cai, K.; Shi, J.; Yu, J.; Qin, Q. H. Dynamic Behavior of a Rotary Nanomotor in Argon Environments. *Sci. Rep.* **2018**, *8*, 3511.
(16) Wang, B.; Kra´l, P. Chemically Tunable Nanoscale Propellers of Liquids. *Phys. Rev. Lett.* **2007**, *98*, 266102.
(17) Barreiro, A.; Rurali, R.; Hernández, E. R.; Moser, J.; Pichler, T.; Forró, L.; Bachtold, A. Subnanometer Motion of Cargoes Driven by Thermal Gradients Along Carbon Nanotubes. *Science* **2008**, *320*, 775-778.
(18) Geng, H. Z.; Kim, K. K.; Lee, K.; Kim, G. Y.; Choi, H. K.; Lee, D. S.; An, K. H.; Lee, Y. H. Dependence of Material Quality on Performance of Flexible Transparent Conducting Films with Single-Walled Carbon Nanotubes. *NANO: Brief Rep. Rev.* **2008**, *2*, 157-167.
(19) Mei, T.; Xiang, D.; Mayer, D. A Crucial Step for Molecular-Scale Electronics: A Stable and Reversible Single-Molecule Switch. *Natl. Sci. Rev.* **2017**.
(20) Chen, J.; Wang, J.; Zhang, G.; Wu, Q.; Wang, D. Facile Fabrication of Nanostructured Cerium-Manganese Binary Oxide

for Enhanced Arsenite Removal from Water. *Chem. Eng. J.* **2018**, *334*, 1518-1526.
(21) Popov, V. N. Carbon Nanotubes: Properties and Application. *Mater. Sci. Eng.: R: Rep.* **2004**, *43*, 61-102.
(22) Liu, Y.; Wang, Q.; Wu, T.; Zhang, L. Fluid Structure and Transport Properties of Water inside Carbon Nanotubes. *J. Chem. Phys.* **2005**, *123*, 234701.
(23) Zou, J.; Ji, B.; Feng, X.; Gao, H. Self-Assembly of Single-Walled Carbon Nanotubes into Multiwalled Carbon Nanotubes in Water: Molecular Dynamics Simulations. *Nano Lett.* **2006**, *6*, 430-434.
(24) Guo, X.; Su, J.; Guo, H. Electric Field Induced Orientation and Self-Assembly of Carbon Nanotubes in Water. *Soft Matter* **2012**, *8*, 1010-1016.
(25) Rahman, M. M.; Chowdhury, M. M.; Alam, M. K. Rotating-Electric-Field-Induced Carbon-Nanotube-Based Nanomotor in Water: A Molecular Dynamics Study. *Small* **2017**, *13*, 1603978.
(26) Fu, Z.; Liang, D.; Jiang, S.; Zhao, P.; Han, K.; Xu, Z. Molecular Dynamics Simulation of Y-Type Nanomotors with Different Angles in Aqueous Solution. *AIP Adv.* **2019**, *9*, 115008.
(27) Iijima, S.; Ajayan, P. M.; Ichihashi, T. Growth Model for Carbon Nanotubes. *Phys. Rev. Lett.* **1992**, *69*, 3100-3103.
(28) Nagy, P.; Ehlich, R.; Bir´o, L. P.; Gyulai, J. Y-Branching of Single Walled Carbon Nanotubes. *Appl. Phys. A: Mater. Sci. Process.* **2000**, *70*, 481-483.
(29) Biró, L. P.; Ehlich, R.; Osváth, Z.; Koós, A.; Horváth, Z. E.; Gyulai, J.; Nagyc, J. B. From Straight Carbon Nanotubes to Y-Branched and Coiled Carbon Nanotubes. *Diamond Relat. Mater.* **2002**, *11*, 1081-1085.
(30) Graovac, A.; László, I.; Pisanski, T. Shape Analysis of Carbon Nanotube Junctions. *MATCH Commun. Math. Co.* **2009**, *60*, 917-926.
(31) Zsoldos, I. Planar Trivalent Polygonal Networks Constructed from Carbon Nanotube Y-Junctions. *J. Geom. Phys.* **2011**, *61*, 37-45.
(32) Hess, B.; Kutzner, C.; Spoel, D. V. D.; Lindahl, E. Gromacs 4: Algorithms for Highly Efficient, Load-Balanced, and Scalable Molecular Simulation. *J. Chem. Theory Comput.* **2008**, *4*, 435-447.
(33) Hummer, G.; Rasaiah, J. C.; Noworyta, J. P. Water Conduction through the Hydrophobic Channel of a Carbon Nanotube. *Nature* **2001**, *414*, 188-190.
(34) Gong, X.; Li, J.; Lu, H.; Wan, R.; LI, J.; Hu, J.; Fang, H. A Charge-Driven Molecular Water Pump. *Nat. Nanotechnol.* **2007**, *2*, 709-712.
(35) Zhou, X.; Lu, H. The Structure and Dynamics of Water inside Armchair Carbon Nanotube. *Chinese Phys.* **2007**, *16*, 335-339.
(36) Wan, R.; Lu, H.; Li, J.; Bao, J.; Hu, J.; Fang, H. Concerted Orientation Induced Unidirectional Water Transport through Nanochannels. *Phys. Chem. Chem. Phys.* **2009**, *11*, 9898-9902.
(37) Gong, X.; Li, J.; Xu, K.; Wang, J.; Yang, H. A Controllable Molecular Sieve for Na+ and K+ Ions. *J. Am. Chem. Soc.* **2010**, *132*, 1873.
(38) Wu, K.; Zhou, B.; Xiu, P.; Qi, W.; Wan, R.; Fang, H. Kinetics of Water Filling the Hydrophobic Channels of Narrow Carbon Nanotubes Studied by Molecular Dynamics Simulations. *J. Chem. Phys.* **2010**, *133*, 204702.
(39) Darden, T.; York, D.; Pedersen, L. Particle Mesh Ewald: An N · Log(N) Method for Ewald Sums in Large Systems. *J. Chem. Phys.* **1993**, *98*, 10089-10092.
(40) Bratko, D.; Daub, C. D.; Leung, K.; Luzar, A. Effect of Field Direction on Electrowetting in a Nanopore. *J. Am. Chem. Soc.* **2007**, *129*, 2504-2510.
(41) Xu, Z.; Hu, G.-H.; Wang, Z.-L.; Zhou, Z.-W. Water Structures inside and Outside Single-Walled Carbon Nanotubes under Perpendicular Electric Field. *Appl. Math. Mech.* **2014**, *35*, 1-12.
(42) Zasetsky, A. Y. Dielectric Relaxation in Liquid Water: Two Fractions or Two Dynamics? *Phys. Rev. Lett.* **2011**, *107*, 117601.
(43) Winarto; Takaiwa, D.; Yamamoto, E.; Yasuoka, K. Separation of Water-Ethanol Solutions with Carbon Nanotubes and Electric Fields. *Phys. Chem. Chem. Phys.* **2016**, *18*, 33310-33319.

TOC graphic:

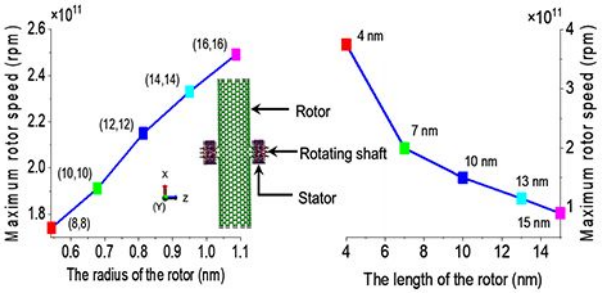

The nanomotor model in the figure consists of three parts: rotor, stator and rotating shaft. As the rotor radius enlarges, the maximum rotational speed of the rotor increases. However, as the length of the motor rotor extends, the maximum rotational speed of the rotor decreases.